

Performance Evaluation of a Vector-Tracking-Loop for GNSS Jamming Effect Mitigation Under Static and Dynamic Conditions

Wang-Seong Cheon¹, Gun-Hoon Ji², Jong-Hoon Won^{1†}

¹Department of Electrical Engineering, Inha University, Incheon 22212, Korea

²Department of Electronics Engineering, Inha University, Incheon 22212, Korea

ABSTRACT

Since the global positioning system receivers on the surface of the Earth use satellite signals sent from a remote distance and the intensity of received signals is weak, they are vulnerable to jamming. This paper implements a vector-tracking loop (VTL)-based global navigation satellite system (GNSS) receiver algorithm as an anti-jamming technique and compares the performance of VTL-based receivers with that of scalar-tracking loop (STL) that is used in general GNSS receivers at various jamming environments and a vehicle's dynamics. The simulation results shows that VTL is more robust against jamming than STL in all operating environments.

Keywords: GPS receiver, anti-jamming, vector tracking loop, dynamic conditions

1. INTRODUCTION

The global navigation satellite system (GNSS) in the world led by global positioning system (GPS) in the USA is a positioning system that determines a position of receiver by measuring a distance between satellite and receiver. It has been usefully employed in military and private areas to provide time and location information. The GNSS has an advantage that can be used globally. However, since it transmits signals remotely from approximately 20,000 km above the earth's surface, reception sensitivity of receivers located around the ground is very weak, which is characterized by fundamental vulnerability to jamming (Chen et al. 2014).

As the dependence on navigation solutions of satellite navigation systems and utilization areas have increased in various fields, jamming cases have also increased. If GNSS signals are jammed, convenient services or functions may be disrupted or confused, resulting in inconvenience in

daily living even up to risk consequences. Thus, various anti-jamming techniques have been investigated to overcome this (Dovis 2015).

The vector-tracking loop (VTL) is known as one of the most advanced receiver algorithms for GNSS signal tracking developed up until now. Conventional receivers have a two-step processing procedure: independent tracking of satellite signals at different channels, and calculating user solution through the use of all tracking results. In contrast, VTL employs a one-step processing procedure that a single central Kalman filter tracks all satellite signals simultaneously and calculates user position and velocity (Lashley 2009). That is, VTL calculates a numerically controlled oscillator (NCO) input value of individual tracking channel using the navigation filter results in contrast with the general scalar-tracking loop (STL) that calculates an NCO input value independently from the individual signal tracking channel. This is a method to update individual channels by sharing information between channels using the fact that signal's phase and frequency is a function of position and velocity of receiver and satellite (Lashley & Bevly 2009). The basic concept of VTL was introduced by Copps et al. (1980) for the first time. Then, this algorithm was named as the vector delay lock loop (VDLL) algorithm by Spilker (1995, 1996) and

Received Dec 28, 2017 Revised July 02, 2018 Accepted July 08, 2018

†Corresponding Author

E-mail: jh.won@inha.ac.kr

Tel: +82-32-860-7406 Fax: +82-32-863-5822

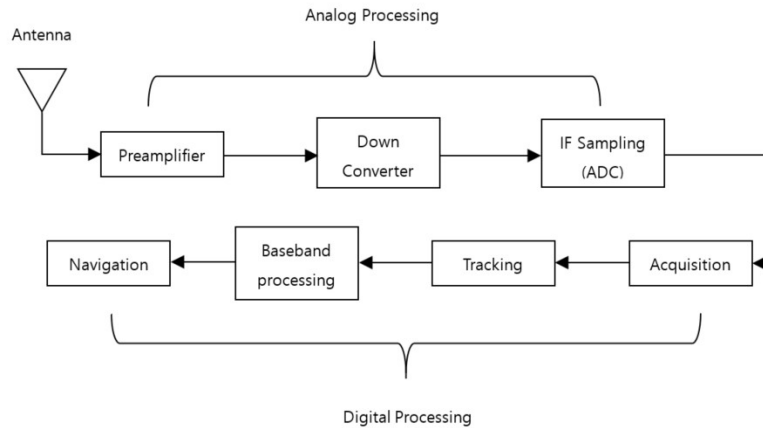


Fig. 1. GNSS receiver architecture.

known to the public.

The advantages of VTL over STL are as follows: It has more robustness against interference and jamming as well as lower carrier-to-noise ratio (C/N₀), and resolves signal failure and has an ability to re-acquire blocked signals immediately. In addition, it is known to be more robust to track the dynamic state of receiver and possible to acquire 3 to 5 dB gain through the efficient channel interaction (Won et al. 2012). On the other hand, VTL has the following major drawbacks that the amount of calculation to be processed is large and complex, and instability of the total tracking channels increases when errors occur at one channel.

The performance comparison between VTL and STL algorithms was conducted in a limited environment for some models (Petovello & Lachapelle 2006, Lashley et al. 2010). Regarding the algorithm implementation, Pany et al. (2005) implemented VDLL and vector frequency lock loop by software, and proved better performance than DLL/FLL at scenarios where visibility was low. Petovello & Lachapelle (2006) compared and analyzed the three Kalman filter algorithms at STL and VTL modes through experiments. Chen et al. (2014) employed adaptive iterated extended Kalman filter at VTL thereby estimating the observation noise of each loop by the noise statistical estimator. Benson (2007) proved that the noise resistance capability of VDLL was more robust than that of general receivers numerically through simulations. Song et al. (2013) presented the comparison results of navigation error between STL-and VTL-based receivers in the continuous-wave (CW) radio jamming signals.

The above studies mainly analyzed performance advantages of VTL over STL at general environments without jamming or conducted the comparison limitedly considering the jamming effect. However, it is necessary to analyze the performance advantages of VTL over STL quantitatively in

environments with various types of jamming sources and sizes.

The present paper compares and analyzes the performance of anti-jamming characteristics against various jamming sources using VTL technique quantitatively with that of conventional STL technique at static and dynamic environments.

This paper is organized as follows. In Section 2, the structure of VTL algorithm is compared with the structure of STL algorithm used in the conventional receivers and comparison results are explained. In Section 3, the performance of VTL and STL at various jamming environments are compared and analyzed through numerical simulations at static and dynamic environments. Finally, Section 4 finishes with Conclusion.

2. GNSS RECEIVER SIGNAL TRACKING LOOP

2.1 Structure of Conventional Receivers

A GNSS receiver is a device that receives satellite signals through antennas and then calculates the signals in the processor thereby providing position, velocity, and timing solution to users. Fig. 1 shows the structure of conventional GNSS receiver. First, an antenna receives GNSS satellite signal. The received GNSS signal is amplified by the radio frequency front-end (RF-FE). Then, the carrier frequency is lowered so it is converted to an intermediate frequency. The analog-to-digital converter at the last stage of RF-FE converts analog signals to digital signal samples. After this, signal processing is mostly done by software using the digital signal processing technique in the digital processing unit.

Signal acquisition at the beginning of digital processing means that a receiver estimates the Doppler shift and initial

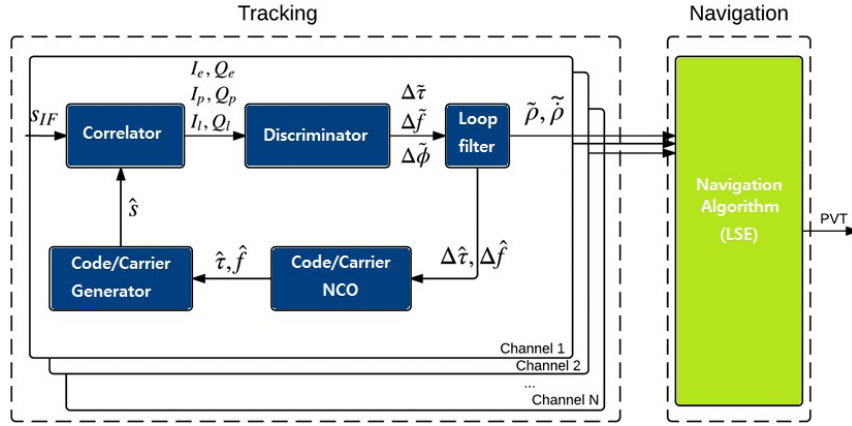


Fig. 2. Algorithm of scalar tracking loop.

code delay of satellite signals approximately. Signal tracking is a process that a receiver acquires code delay, Doppler, and carrier wave phase information more precisely. The baseband processing unit is used to demodulate a navigation message and calculate a pseudorange. Finally, the navigation unit is used to calculate a receiver's position based on the ephemeris and pseudorange.

2.2 Scalar-Tracking Loop

Signal tracking is a process that estimate a fine value of signal parameter truth (SPT) based on signal acquisition result and previous estimation information. Generally, SPT refers to code delay, Doppler, and carrier phase.

Fig. 2 shows the block diagram of STL. As shown in the figure, the signal tracking loop is a closed loop consisting of correlator, discriminator, loop filter, and NCO. In the figure, (I_e, Q_e) , (I_p, Q_p) , and (I_l, Q_l) refer to in-phase (I) and quadrature (Q) outputs at early, prompt, and late correlators with regard to incoming IF signals. $(\Delta\tilde{\tau}, \Delta\tilde{f}, \Delta\tilde{\phi})$ is a discriminator output, which refers to error values of code delay, Doppler frequency, and initial carrier phase. $(\tilde{\rho}, \tilde{\rho})$ is a converted value of the loop filter's output value, which refers to an error of pseudorange and pseudorange rate, respectively. $(\Delta\hat{\tau}, \Delta\hat{f})$ is an NCO's input value, which refers to an error estimate of code delay and Doppler frequency, respectively. $(\hat{\tau}, \hat{f})$ is a code and carrier wave signal generator's input value, which refers to a newly predicted/estimated code delay and Doppler frequency value.

In STL, SPT is estimated and then navigation solution is calculated based on the estimated SPT. As shown in the figure, the channels are separated one another, and information calculated at one channel does not influence signal tracking of other channels at all. That is, the channels are operated individually and independently.

2.3 Vector-Tracking Loop

In this section, VTL algorithm is explained with a series of equations, which will be the foundation of VTL receiver simulation in the next sections. The general VTL structure is described, and a method of how to design VTL is explained.

Fig. 3 shows the block diagram of VTL. Initially, VTL calculates a navigation solution using a general of the extended Kalman filter, and then updates NCO input values, which are SPT estimates. According to the configuration of the local filter in VTL, discriminator values or baseband signal values may be used directly (Won et al. 2012).

The Kalman filter of the navigation in the VDFLL structure is described to explain the update process of the state vector in VTL structure in detail. First, the state transition model is presented in Eqs. (1) and (2).

$$X_{k+1} = F \cdot X_k + w_k \quad (1)$$

$$\begin{bmatrix} x \\ y \\ z \\ \dot{x} \\ \dot{y} \\ \dot{z} \\ t \\ \dot{t} \end{bmatrix}_{k+1} = \begin{bmatrix} 1 & 0 & 0 & T & 0 & 0 & 0 & 0 \\ 0 & 1 & 0 & 0 & T & 0 & 0 & 0 \\ 0 & 0 & 1 & 0 & 0 & T & 0 & 0 \\ 0 & 0 & 0 & 1 & 0 & 0 & 0 & 0 \\ 0 & 0 & 0 & 0 & 1 & 0 & 0 & 0 \\ 0 & 0 & 0 & 0 & 0 & 1 & 0 & 0 \\ 0 & 0 & 0 & 0 & 0 & 0 & 1 & T \\ 0 & 0 & 0 & 0 & 0 & 0 & 0 & 1 \end{bmatrix} \begin{bmatrix} x \\ y \\ z \\ \dot{x} \\ \dot{y} \\ \dot{z} \\ t \\ \dot{t} \end{bmatrix}_k + \begin{bmatrix} w_x \\ w_y \\ w_z \\ w_{\dot{x}} \\ w_{\dot{y}} \\ w_{\dot{z}} \\ w_t \\ w_{\dot{t}} \end{bmatrix}_k \quad (2)$$

where

F : state transition matrix

$[x, y, z]$: user position in ECEF coordinates

$[\dot{x}, \dot{y}, \dot{z}]$: user velocity in ECEF coordinates

t : clock offset

\dot{t} : clock drift

T : integration time

w_k : process noise

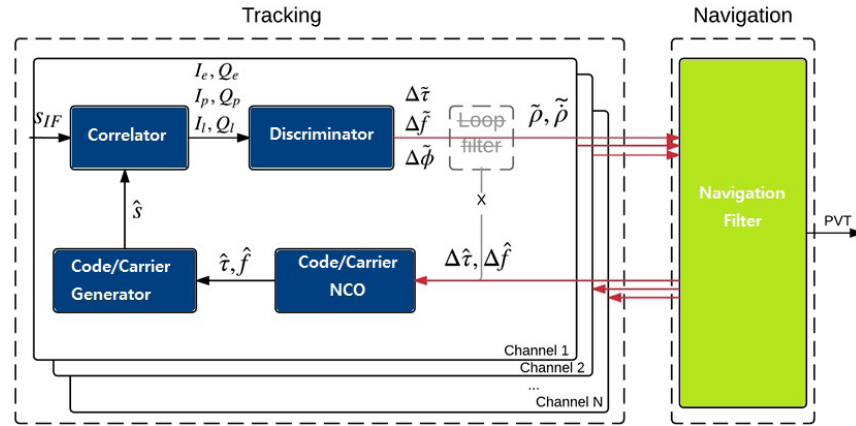


Fig. 3. Algorithm of vector tracking loop.

As presented in the state vector configuration in Eq. (2), the state vector is defined by user's position, velocity, clock offset, and clock drift. The pseudorange measurement of the satellite with considering the absence of the noise effect can be acquired by the range between user and satellite plus the receiver clock error. Since the pseudorange is a non-linear function, linearization task is needed as follows (So et al. 2010):

$$\begin{aligned} \rho_i &= r_u^i + ct_u \\ &= \sqrt{(x_i - x_u)^2 + (y_i - y_u)^2 + (z_i - z_u)^2} + ct_u \\ &= \varphi(x_u, y_u, z_u, t_u) \end{aligned} \tag{3}$$

$$\begin{aligned} \delta\rho_i &= \frac{\partial\varphi}{\partial x_u} \delta x_u + \frac{\partial\varphi}{\partial y_u} \delta y_u + \frac{\partial\varphi}{\partial z_u} \delta z_u + \frac{\partial\varphi}{\partial t_u} \delta t_u \\ &= \frac{x_i - \hat{x}_u}{r_u^i} \delta x_u + \frac{y_i - \hat{y}_u}{r_u^i} \delta y_u + \frac{z_i - \hat{z}_u}{r_u^i} \delta z_u - c\delta t_u \end{aligned} \tag{4}$$

where

- ρ_i : pseudorange from the i -th satellite to user
- r_u^i : i -th true range from user to satellite
- t_u : receiver clock offset
- $[a_{x_i}^i, a_{y_i}^i, a_{z_i}^i]$: vector component from user u to satellite i

Based on the linearized equation above, the measurement residual vector can be expressed as follows:

$$\Delta Z_k = H \cdot \Delta X_k + v_k \tag{5}$$

$$\begin{aligned} \begin{bmatrix} \delta\hat{\rho}_1 \\ \vdots \\ \delta\hat{\rho}_s \\ \vdots \\ \delta\hat{\rho}_1 \\ \vdots \\ \delta\hat{\rho}_{s-k} \end{bmatrix} &= \begin{bmatrix} (\Delta\hat{\rho}_1 + \hat{\rho}_1) - \hat{\rho}_1^- \\ \vdots \\ (\Delta\hat{\rho}_s + \hat{\rho}_s) - \hat{\rho}_s^- \\ \vdots \\ (\Delta\hat{\rho}_1 + \hat{\rho}_1) - \hat{\rho}_1^- \\ \vdots \\ (\Delta\hat{\rho}_s + \hat{\rho}_s) - \hat{\rho}_s^- \end{bmatrix} \\ &= - \begin{bmatrix} e_{u1,x} & e_{u1,y} & e_{u1,z} & 0 & 0 & 0 & -c & 0 \\ \vdots & \vdots \\ e_{us,x} & e_{us,y} & e_{us,z} & 0 & 0 & 0 & -c & 0 \\ 0 & 0 & 0 & e_{u1,x} & e_{u1,y} & e_{u1,z} & 0 & -c \\ \vdots & \vdots \\ 0 & 0 & 0 & e_{us,x} & e_{us,y} & e_{us,z} & 0 & -c \end{bmatrix} \begin{bmatrix} \delta x \\ \delta y \\ \delta z \\ \delta \hat{x} \\ \delta \hat{y} \\ \delta \hat{z} \\ \delta t \\ \delta \hat{t} \end{bmatrix}_k + \begin{bmatrix} v_x \\ v_y \\ v_z \\ v_{\hat{x}} \\ v_{\hat{y}} \\ v_{\hat{z}} \\ v_t \\ v_{\hat{t}} \end{bmatrix}_k \end{aligned} \tag{6}$$

where

- v_k : observation noise
- $\tilde{\rho}$: measured pseudorange
- $\Delta\tilde{\rho}$: discriminator output
- $\hat{\rho}$: pseudorange estimate
- $\delta\tilde{\rho} = \Delta\tilde{\rho} + \tilde{\rho} - \hat{\rho}$: pseudorange error
- H : observation model matrix
- $e_{u,i}$: line-of-sight (LOS) unit vector

The measurement residual vector is composed of difference between value adding the measured pseudorange ($\tilde{\rho}$) to the discriminator output ($\Delta\tilde{\rho}$), and the pseudorange estimate ($\hat{\rho}$).

After this, the code delay and Doppler frequency are updated through the navigation process in Fig. 3 using the above defined VDFLL Kalman filter. In order to calculate the measurement residual first, the pseudorange and pseudorange-rate measurements are calculated through the code delay & Doppler frequency obtained from the discriminator previously, and their pseudorange rate, and then each estimate can be calculated via Eqs. (7-11) through the state vector's predicted value.

$$\hat{X}_{k+1}^- = F \cdot \hat{X}_k^+ : \text{prior range estimation} \tag{7}$$

$$\tilde{\rho} + \Delta\tilde{\rho} = (\tilde{\tau} + \Delta\tilde{\tau}) \cdot \frac{c}{f_{code}} : \text{pseudorange measurement} \tag{8}$$

$$\tilde{\rho} + \Delta\tilde{\rho} = (f_{Dopp} + \Delta f_{Dopp}) \cdot \frac{c}{f_{carr}} : \text{pseudorange-rate measurement} \tag{9}$$

$$\hat{\rho}^- \approx (x_s - \hat{x}_u^-) \cdot e_{us} + c \cdot t_u : \text{pseudorange estimation } (e_{us} = \frac{x_s - \hat{x}_u^-}{|x_s - \hat{x}_u^-|}) \tag{10}$$

$$\hat{\rho}^- \approx (\dot{x}_s - \dot{\hat{x}}_u^-) \cdot e_{us} + c \cdot \dot{t}_u : \text{pseudorange-rate estimation } (e_{us} = \frac{x_s - \hat{x}_u^-}{|x_s - \hat{x}_u^-|}) \tag{11}$$

The measurement residual is calculated by a difference between actual pseudorange and the estimate value as presented in Eq. (12).

$$\Delta Z = \begin{bmatrix} (\Delta\hat{\rho} + \tilde{\rho}) - \hat{\rho}^- \\ (\Delta\tilde{\rho} + \tilde{\rho}) - \hat{\rho}^- \end{bmatrix} : \text{Measurement residual} \quad (12)$$

Following this, the position error is estimated which is then used to calculate the position navigation solution. The covariance prediction is calculated for the position error as presented in Eq. (13). Using this, Kalman gain is calculated through Eq. (14).

$$P_{k+1}^- = FP_k^+ F^T + Q : \text{Covariance matrix a prior prediction} \quad (13)$$

$$K_{k+1} = P_{k+1}^- H_{k+1}^T (H_{k+1} P_{k+1}^- H_{k+1}^T + R_{k+1})^{-1} : \text{Optimal Kalman Gain} \quad (14)$$

Using the covariance prediction and Kalman gain calculated via Eqs. (13) and (14), the navigation solution error is estimated, and then navigation solution is updated again as presented in Eqs. (15) and (16).

$$\Delta X_{k+1} = K_{k+1} \cdot \Delta Z_{k+1} : \text{Update state correction} \quad (15)$$

$$\hat{X}_{k+1}^+ = \hat{X}_{k+1}^- + \Delta X_{k+1} : \text{Position update} \quad (16)$$

The pseudorange error is calculated through the system matrix using the position error calculated via Eq. (15), and newly estimated pseudorange is calculated using the updated navigation solution.

$$\begin{bmatrix} \Delta\hat{\rho} \\ \Delta\hat{\dot{\rho}} \end{bmatrix} = H \cdot \Delta X : \text{pseudorange \& rate error estimation} \quad (17)$$

$$\hat{\rho}_s^+ = \sqrt{(x_s - x_u^+)^T (x_s - x_u^+)} + c \cdot t_u^+ : \text{pseudorange estimation} \quad (18)$$

$$\hat{\dot{\rho}}_s^+ = \sqrt{(\dot{x}_s - \dot{x}_u^+)^T (\dot{x}_s - \dot{x}_u^+)} + c \cdot \dot{t}_u^+ : \text{pseudorange-rate estimation} \quad (19)$$

Through the above calculated values, the error of code delay & Doppler frequency, which is a tracking control input of VTL, is calculated via Eqs. (20) and (21), which are defined as the NCO inputs.

$$\Delta\hat{t} = (\Delta\hat{\rho} + \hat{\rho}^+ - \tilde{\rho}) \cdot \frac{f_{code}}{c} : \text{Code NCO input} \quad (20)$$

$$\Delta\hat{f} = (\Delta\hat{\rho} + \hat{\rho}^+ - \tilde{\rho}) \cdot \frac{f_{carr}}{c} : \text{Carrier NCO input} \quad (21)$$

After this, the code delay & Doppler frequency are estimated in the code/carrier NCO using the NCO input values of Eqs.

(20) and (21).

$$\hat{t} = \hat{t} + \Delta\hat{t} : \text{Code NCO} \quad (22)$$

$$\hat{f} = \hat{f} + \Delta\hat{f} : \text{Carrier NCO} \quad (23)$$

Finally, the estimated values are entered to the tracking loop feedback through the generator thereby calculating signals where the code delay & Doppler frequency are updated.

As described in the above, VTL-based GPS receiver consists of a single loop where the navigation calculation and signal tracking are combined by utilizing position information of satellite and receiver obtained from the satellite measurements. In addition, the signal tracking unit is also implemented as a form of local Kalman filter during VTL implementation thereby acquiring additional gain by adjusting the bandwidth of the signal tracking filter efficiently (Won et al. 2012).

A previous study reported that 2 to 3 dB gain from the efficient use of local Kalman filter for signal tracking and additional gain of around 5 dB due to the channel interaction by satellite layout can be obtained, and therefore totally about 7 dB gain can be obtained when using VTL compared to that of STL (Won & Eissfeller 2010, Won et al. 2011). That is, a VTL-based receiver is more advantageous in tracking weak signals and more robust in radio jamming environments than that of STL-based receiver.

2.4 Radio Interference Sources

Radio interference in communication systems is defined as undesirable energy effect due to one or more cases of emission, radiation, and induction in the wireless communication system (Samson 2014). Generally, radio interference in the GNSS band refers to all RF transmission signals within the band that degrades the GNSS receiver performance. All RF signals generated in electronic systems and electrical communications operated at a band which is the same or adjacent band with the GNSS signal band may cause radio interference to the GNSS system. Radio interference can be classified in various ways for example intentional or non-intentional radio interference, or GNSS system or non-GNSS system radio disturbance.

The GNSS radio interference assumed in this study followed the technical classification according to the signal type: Continuous Wave Interference (CWI), chirp interference, pulse interference, Matched Spectrum Interference (MSI), and Band Limited White Interference (BLWI). The individual characteristics are well summarized in Kaplan & Hegarty (2006).

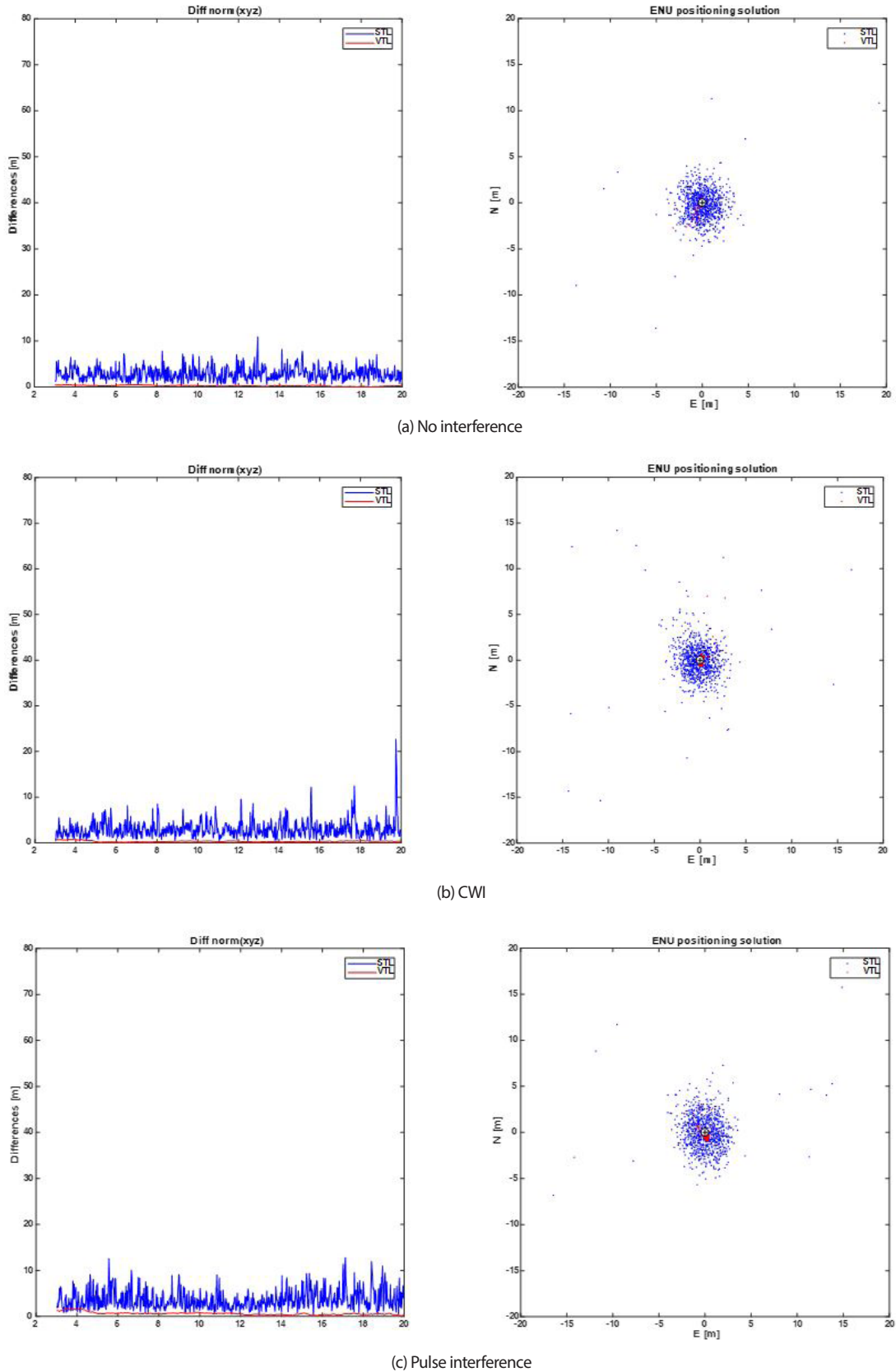
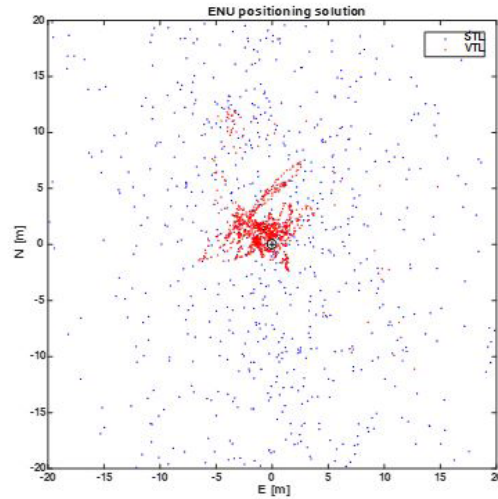
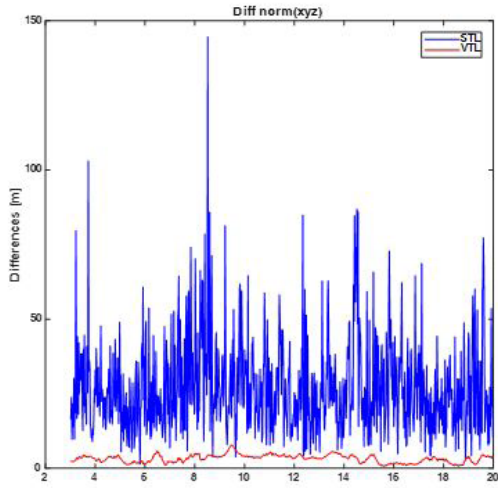
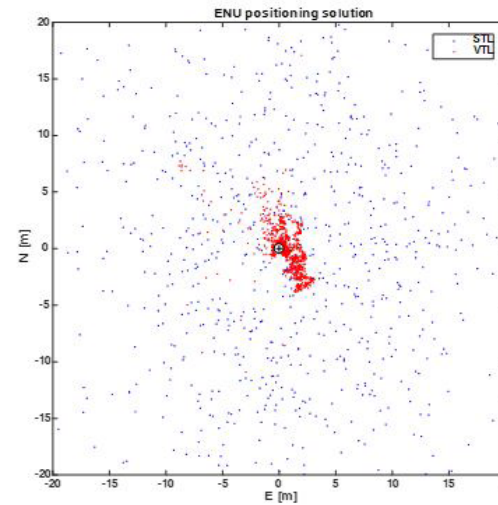
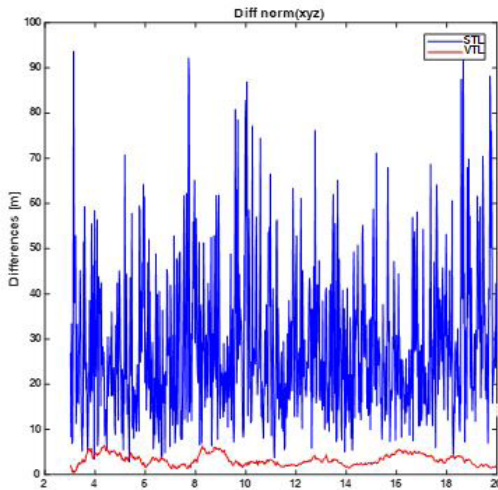


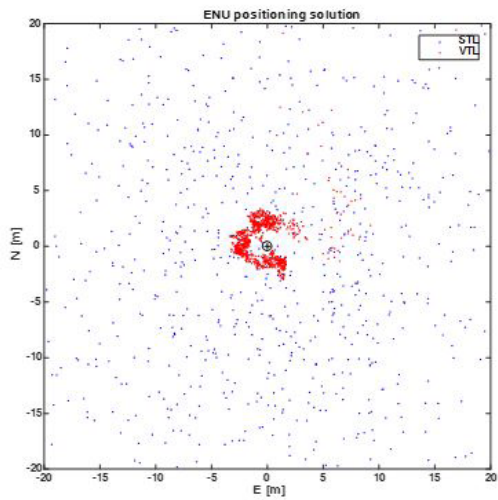
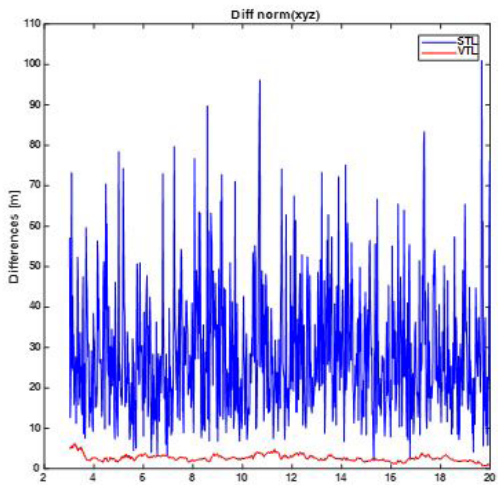
Fig. 4. Positioning result based on scalar tracking and vector tracking with (static scenario) under various interference scenarios ($J/S @ 35\text{dB}$).



(d) Chirp interference



(e) MSI



(f) BLWI

Fig. 4. Continued

3. SIMULATION CONFIGURATION

This paper compares the performance of STL and VTL receiver algorithms through numerical simulations at various jamming environments and dynamic environment setup of receivers. To do this, the aforementioned receiver algorithms were implemented by MATLAB. This configuration of the simulation is as follows. First, GNSS data and user data that are suitable for values (time interval, user trajectory, etc.) set in the signal generation process through the signal simulator are fetched. Then using the data, the SPT values are calculated and these values are assigned to corresponding structures. After this, a base band signal is generated using a difference between a value calculated at the receiver through the receiver simulator and the generated SPT value, followed by performing acquisition and tracking processes. Here, STL or VTL method can be chosen during tracking according to the value set at the receiver previously, and depending on the selected method, a process of tracking and navigation is applied differently. In addition, jamming effects were analyzed by modeling various radio interference signals and applying them to the receiver simulator.

3.1 Static Simulation at Various Jamming Environments

Assuming there was no radio interference, the effectiveness of VTL-based receiver was verified through simulations. Since VTL employs individual channel update through efficient information sharing between channels in contrast with STL in which analyses are convenient in the LOS domain due to no information sharing between channels, geometric layout state of all visible satellites and receivers affect the performance of signal tracking and navigation solution. Thus, analyses on entire position errors of navigation solution are more useful to compare the two algorithms than analyses on tracking information of individual channel. Thus, the performances of two algorithms were compared via the comparison of positioning error obtained by the process of STL and VTL while changing the motion state of user at various radio interference environments.

Fig. 4 shows the navigation solution processed with STL and VTL during static case in two-dimensional plane and three-dimensional positioning error according to time elapse for five types of radio interference signals. In Fig. 4, a scale is set differently to show the positioning error visibly for the comparison of the results between STL and VTL. The CWI, chirp interference, pulse interference, MSI, and BLWI signals were modeled and applied to simulations. The navigation solution processing results of STL and VTL are displayed in a single graph with blue color of STL and red color of VTL.

For a radio interference environment used in the simulation, the CWI phase in the CWI environment was set to 0, and the chirp rate in the chirp interference environment was set to 100 MHz, and sweep time was set to 10 ms. The pulse duration, pulse rate, and pulse duty cycle in the pulsed interference environment were set to 10 μ sec, 3,000 pp/s, and 3%, respectively. For MSI, additional setup was not needed since it was the same with the existing spectrum setup, and for BLWI, interference bandwidth was set to 2.046 MHz. For CWI, difference was set to 0 to match the phase with that of C/A code, and for pulsed interference, a duty cycle and pulse per sec were set to 5% or smaller and 3,000 according to the distance measurement equipment / tactical air navigation principle. The jamming to signal ratio (J/S) in all of the five radio interference environments was set to 35 dB to test the increase in positioning error by different jamming types for the same jamming power. As shown in Fig. 4, VTL reduced the navigation solution error much more significantly than that of STL.

Tables 1 and 2 and Fig. 5 present the overall simulation results that compare positioning error while changing only J/S of each interference signal with 5 dB increment from 15 dB to 35 dB at the same static case scenario with the previous simulation. The given tables summarize positioning errors and standard deviations numerically for each scenario. Fig. 5a shows the RMS positioning error for each scenario by dividing J/S from 15 dB to 35 dB with regard to each of STL and VTL, and Fig. 5b shows how the errors are displayed according to a jammer. The above figures verified that the jamming effects of chirp interference, MSI, and BLWI became larger as the jamming power was larger than those of CWI and pulsed interference. This result mean that jamming of chirp interference was the most efficient jamming that covers the wide area followed by MSI and BLWI for the same J/S from the jammer's viewpoint, which was consistent with the existing study results about jamming resistance quality factor (Kaplan & Hegarty 2006). As summarized in the tables, the navigation performance using VTL was better than those using STL even in the radio interference environments.

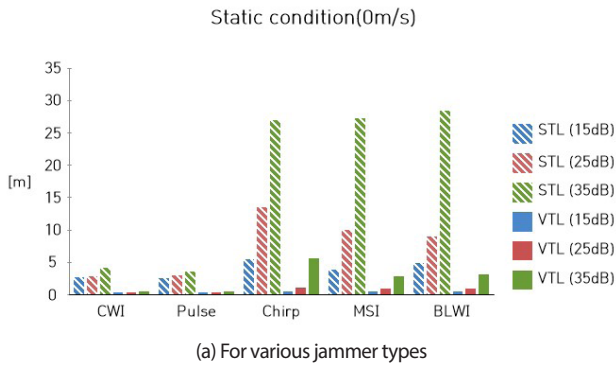
Fig. 6 shows the RMS positioning error of VTL compared to that of STL when J/S of each interference signal is changed from 15 dB to 35 dB using the above simulation results. When 35 dB power was applied in each of the jamming environments, a positioning error using VTL was reduced by 93.52% compared to that using STL in no interference environment, 91.21% in CWI, 89.53% in pulse interference, 79.23% in chirp, 90.03% in MSI, and 89.15% in BLWI, indicating that the performance was improved. Thus, performances of VTL-based receiver were better than those of STL-based receiver in all radio interference environments

Table 1. RMS position error.

Type	J/S (dB)						VTL bias (m)					
	No Jamming	15	20	25	30	35	No Jamming	15	20	25	30	35
CWI	2.61	2.692	2.659	2.744	2.749	4.099	0.169	0.251	0.300	0.347	0.338	0.360
Chirp	2.61	5.407	7.056	13.38	14.86	26.9	0.169	0.400	0.661	0.961	1.933	5.586
Pulse	2.61	2.514	2.863	2.9	3.292	3.499	0.169	0.234	0.242	0.260	0.288	0.366
MSI	2.61	3.719	6.083	10.02	16	27.24	0.169	0.402	0.753	0.850	1.638	2.714
BLWI	2.61	4.842	6.684	8.909	16	28.38	0.169	0.358	0.468	0.835	1.669	3.078

Table 2. Standard deviation of the position error.

Type	J/S (dB)						VTL bias (m)					
	No Jamming	15	20	25	30	35	No Jamming	15	20	25	30	35
CWI	1.441	1.352	1.416	1.499	1.404	1.944	0.112	0.118	0.100	0.097	0.094	0.136
Chirp	1.441	2.564	2.291	4.807	8.143	15.66	0.112	0.123	0.308	0.419	1.003	1.304
Pulse	1.441	1.446	1.212	1.326	2.483	2.061	0.112	0.121	0.132	0.115	0.113	0.311
MSI	1.441	2.284	3.001	4.596	9.761	16.21	0.112	0.186	0.339	0.936	1.439	1.209
BLWI	1.441	2.058	3.48	5.057	8.53	15.57	0.112	0.120	0.224	0.483	1.225	0.829



(a) For various jammer types

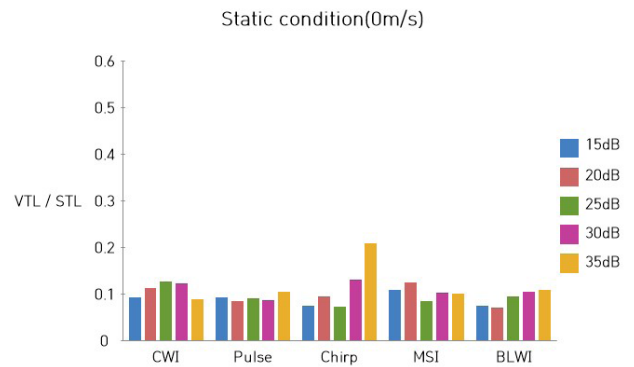
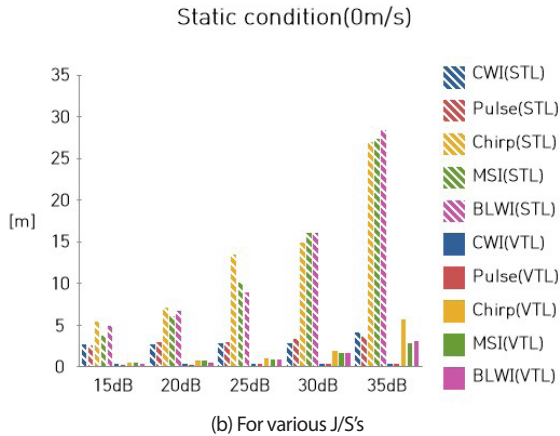


Fig. 6. VTL RMS position error ratio to STL position error (Static scenarios).



(b) For various J/S's

Fig. 5. RMS position errors (static scenarios with J/S).

using simulations.

3.2 Dynamic Simulation at Various Jamming Environments

To analyze performances at dynamic environments, a J/S range was set between 0 dB and 30 dB with 10 dB increment

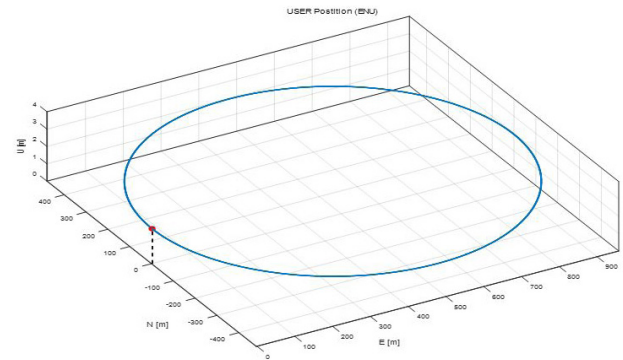


Fig. 7. Generated receiver trajectory.

assuming that only one jamming signal exists. Fig. 7 shows the generated trajectory of the vehicle. The vehicle simulation was assumed to have a uniform circular motion along the dynamic trajectory with velocity of static, 10, 25, and 50 m/s (0, 36, 90, and 180 km/h). The skyplot of the satellite is shown in Fig. 8. Table 3 summarizes this simulation environment data.

Tables 4 and 5 present the navigation errors and standard deviations according to changes in J/S for each velocity

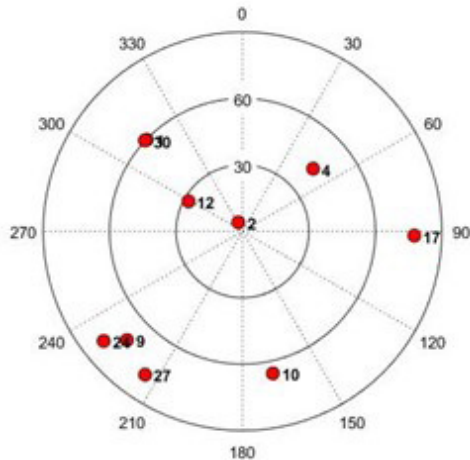


Fig. 8. GPS satellite skyplot.

Table 3. Simulation environment variables.

Variables	Value
Visible satellite number	9
Jammer type	CWI, Chirp, Pulse, MSI, BLWI
J/S range	0-30 dB
Velocity range	0, 10, 25, 50 m/s (0, 36, 90, 180 km/h)

obtained from the simulations. Figs. 9-13 show the RMS positioning error to display comparison results according to a velocity for each jammer after VTL navigation errors are divided by STL navigation errors presented in Tables 4 and 5. Fig. 14 shows the figure that combines Figs. 9-13. Figs. 9-14 verify that positioning error of VTL due to jammer shows better performance than that of STL.

The results of Tables 4 and 5 and Fig 9-13 verify that

navigation errors and standard deviations using VTL were smaller than those using STL overall. In addition, they verify that the effects of chirp interference, MSI, and BLWI jamming are relatively larger than those of CWI and pulse interference, and positioning errors due to jamming become larger in STL as a J/S value is larger at high velocity. In contrast, VTL-based receiver was more robust against all radio interference signals than STL-based receiver. Accordingly, the trend of navigation error rates using VTL and STL at 50 m/s are shown in Figs. 9-13. These results indicated that VTL-based receiver was more robust to jamming than STL-based receiver with regard to all five types of radio interference signals used in the simulations, and it was also more effective against relatively larger effect of jamming.

Fig. 15 shows the comparison of arrival spots at the 3/4 spot of the generated path at CWI jamming whose J/S value is 30 dB with 50 m/s velocity among the navigation results of STL and VTL. The STL, VTL, and true trajectories are marked with blue, red, and black colors, respectively. The figure verifies that VTL trajectory follows the true trajectory very closely, which reveals clearly the performance difference between STL and VTL.

4. CONCLUSIONS

This paper implemented a signal processing algorithm of VTL-based receiver, and performances at a number of dynamic conditions and various jamming environments such as CWI, chirp interference, pulse interference, MSI, and

Table 4. RMS position errors (dynamic scenarios).

Interference type	Velocity (m/s)	J/S	STL Bias (m)			VTL Bias (m)				
			No Jamming	10 dB	20 dB	30 dB	No Jamming	10 dB	20 dB	30 dB
CWI	0		2.610	2.692	2.647	2.749	0.169	0.251	0.300	0.338
	10		2.799	2.739	3.059	3.055	0.424	0.465	0.472	0.841
	25		2.827	2.943	2.961	3.058	0.768	0.814	0.910	1.851
	50		2.840	2.924	3.081	4.280	1.657	1.675	1.853	3.408
Pulse	0		2.610	2.589	2.863	3.292	0.169	0.236	0.242	0.288
	10		2.799	3.797	2.724	2.821	0.424	0.385	0.442	0.433
	25		2.827	3.061	3.667	3.854	0.768	0.901	0.919	0.863
	50		2.840	3.017	2.645	2.764	1.657	1.742	1.671	2.168
Chirp	0		2.610	5.166	7.056	14.860	0.169	0.389	0.661	1.933
	10		2.799	4.543	8.039	20.327	0.424	0.430	0.935	1.866
	25		2.827	3.191	6.460	18.722	0.768	0.804	0.981	1.856
	50		2.840	3.641	7.739	20.774	1.657	1.687	1.976	3.830
MSI	0		2.610	3.624	6.083	16	0.169	0.415	0.753	1.638
	10		2.799	3.310	6.039	16.766	0.424	0.489	0.578	2.051
	25		2.827	3.014	6.711	16.90	0.768	0.846	1.202	2.586
	50		2.840	3.455	7.509	16.524	1.657	1.719	1.780	4.181
BLWI	0		2.610	4.427	6.684	16	0.169	0.352	0.468	1.669
	10		2.799	3.389	3.343	19.933	0.424	0.448	0.610	2.659
	25		2.827	3.838	7.607	17.026	0.768	0.961	0.858	2.695
	50		2.840	3.993	6.905	16.712	1.657	1.651	1.832	3.858

Table 5. Standard deviation of position errors (dynamic scenarios).

Interference type	Velocity (m/s)	J/S	STL Bias (m)			VTL Bias (m)				
			No Jamming	10 dB	20 dB	30 dB	No Jamming	10 dB	20 dB	30 dB
CWI	0		1.441	1.388	1.416	1.404	0.112	0.091	0.100	0.094
	10		1.377	1.565	1.439	3.713	0.136	0.147	0.143	0.564
	25		1.408	1.448	1.372	4.315	0.180	0.160	0.270	1.698
	50		1.727	1.520	1.6	5.597	0.246	0.496	0.523	3.209
Pulse	0		1.441	1.352	1.212	2.483	0.112	0.122	0.339	1.439
	10		1.377	1.960	1.444	1.495	0.136	0.154	0.132	0.125
	25		1.408	1.558	1.883	2.016	0.180	0.170	0.183	0.179
	50		1.727	1.580	1.334	1.419	0.246	0.269	0.326	0.422
Chirp	0		1.441	2.017	2.291	2.483	0.112	0.135	0.339	1.439
	10		1.377	2.336	4.599	13.322	0.136	0.181	0.405	1.964
	25		1.408	1.637	3.566	11.251	0.180	0.220	0.390	1.061
	50		1.727	2.004	4.252	12.156	0.246	0.358	1.401	6.030
MSI	0		1.441	2.249	3.0001	9.761	0.112	0.192	0.224	1.225
	10		1.377	1.681	3.122	8.923	0.136	0.251	0.283	1.008
	25		1.408	1.859	4.271	8.909	0.180	0.240	0.309	1.075
	50		1.727	1.619	3.690	8.709	0.246	0.352	0.529	1.985
BLWI	0		1.441	1.988	1.702	9.761	0.112	0.134	0.224	1.225
	10		1.377	1.863	3.480	11.024	0.136	0.150	0.180	2.171
	25		1.408	2.054	4.199	8.980	0.180	0.182	0.302	1.167
	50		1.727	2.150	3.684	8.754	0.246	0.314	0.484	1.852

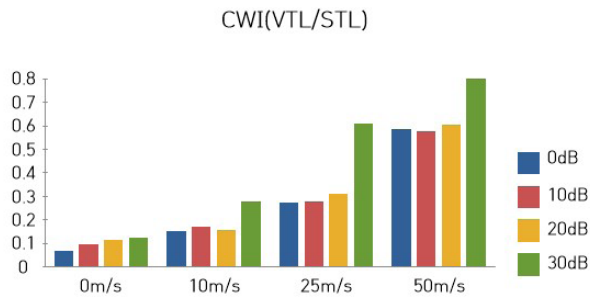


Fig. 9. VTL RMS position error ratio to STL position error (CWI scenarios).

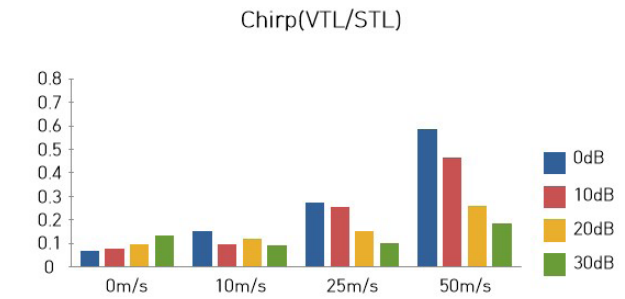


Fig. 11. VTL RMS position error ratio to STL position error (Chirp scenarios).

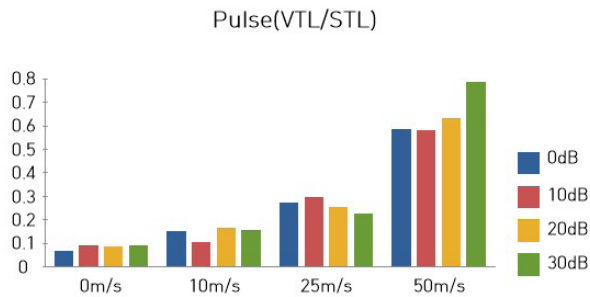


Fig. 10. VTL RMS position error ratio to STL position error (Pulse scenarios).

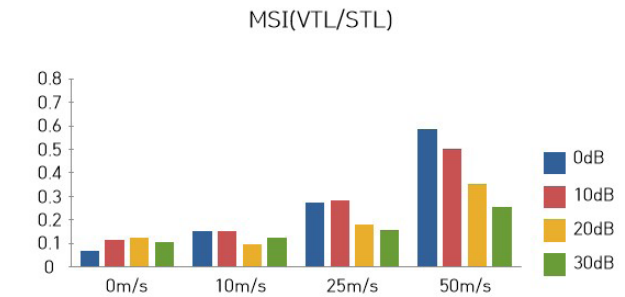


Fig. 12. VTL RMS position error ratio to STL position error (MSI scenarios).

BLWI were compared through simulations with those using conventional STL. The comparison results of navigation errors verified that VTL-based receiver had more J/S gain than that of STL-based receiver even in receiver dynamic conditions as well as better performance similarly even in no-dynamic (static) conditions. Furthermore, the effects of chirp interference, MSI, and BLWI jammers were relatively larger than those of CWI and pulsed interference at both of static

and dynamic conditions. In particular, the analysis results of positioning error rates between VTL and STL in Figs. 9-13 showed that much better performances were revealed in VTL than STL when J/S and dynamic conditions were smaller.

The above simulation results proved the robustness of VTL algorithm implemented in this study at radio interference environments and dynamic conditions. The results in this study are expected to contribute to resolving the jamming

BLWI(VTL/STL)

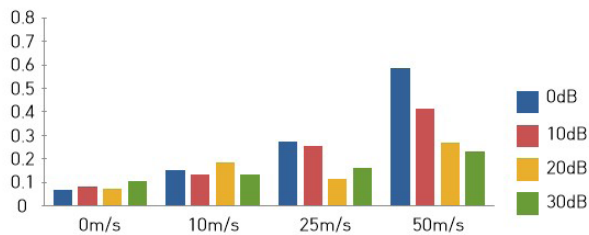


Fig. 13. VTL RMS position error ratio to STL position error (BLWI scenarios).

(VTL/STL)

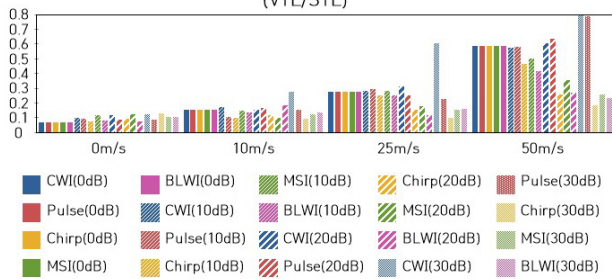


Fig. 14. VTL RMS position error ratio to STL position error (Dynamic scenarios).

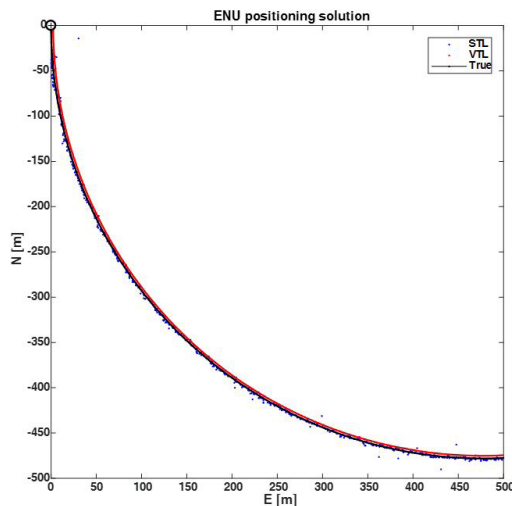


Fig. 15. Comparison of positioning results between scalar tracking loop and vector tracking loop.

problem in the GNSS including GPS.

ACKNOWLEDGMENTS

This study was part of the Space Technology Development Project supported by the National Research Foundation of Korea funded by the Ministry of Science, ICT and Future Planning in 2017 [Project Number: 2017M1A3A9014637].

REFERENCES

Benson, D. 2007, Interference Benefits of a Vector Delay Lock Loop (VDLL) GPS Receiver, in Proceedings of the 63rd Annual Meeting of the Institute of Navigation. Cambridge, April 23 - 25, 2007, Royal Sonesta Hotel, Cambridge, MA, pp.749-756

Chen, X. 2014, Modelling of GNSS Challenged Environment in Semi-Analytical Simulator, Master's Thesis, Institute of Space Technology and Space Applications, University Federal Armed Forces Munich

Chen, X., Wang, X., & Xu, Y. 2014, Performance Enhancement for a GPS Vector-Tracking Loop Utilizing an Adaptive Iterated Extended Kalman Filter, *Sensors*, 14, 23630-23649. <https://doi.org/10.3390/s141223630>

Copps, E. M., Geier, G. J., Fidler, W. C., & Grundy, P. A. 1980, Optimal processing of GPS signals, *Navigation*, 27, 171-182. <https://doi.org/10.1002/j.2161-4296.1980.tb01417.x>

Dovis, F. (eds.), 2015, GNSS Interference Threats and Countermeasures (Boston: Artech House Inc.)

Kaplan, E. D. & Hegarty, C. J. 2006, Understanding GPS: Principles and Applications, 2nd ed. (Boston: Artech House Inc.)

Lashley, M. 2009, Modeling and Performance analysis of GPS vector tracking, PhD thesis, Auburn University

Lashley, M. & Bevly, D. M. 2009, What are vector tracking loops, and what are their benefits and drawbacks?, *Inside GNSS*, May/June 2009, pp.16-21. <https://pdfs.semanticscholar.org/158f/749d32d8946b8904a120519522ef9b45d5e1.pdf>

Lashley, M., Bevly, D. M., & Hung, J. Y. 2010, A valid comparison of vector and scalar tracking loops, *Proc. IEEE PLANS, Position Location and Navigation Symposium*, pp.464-474. <https://doi.org/10.1109/PLANS.2010.5507215>

Pany, T., Kaniuth, R., & Eissfeller, B. 2005, Testing a Vector Delay/Frequency Lock Loop Implementation with the ipex Software Receiver, *Proc. GPS/GNSS Symposium*, pp.1-9

Petovello, M. G. & Lachapelle, G. 2006, Comparison of Vector-Based Software Receiver Implementations With Application to Ultra-Tight GPS/INS Integration, *Proc. the 19th International Technical Meeting of the Satellite Division of The Institute of Navigation (ION GNSS 2006)*, September 26-29, 2006, Fort Worth Convention Center, Fort Worth, TX, pp.1790-1799

Samson, J. 2014, An Introduction to Interference in GNSS-bands, Technical report, European Navigation Conference 2014, At Rotterdam, Holland. <https://doi.org/10.13140/2.1.5042.1762>

- So, H., Lee, T., Jeon, S., Kim, C., Kee, C., et al. 2010, Implementation of a vector-based tracking loop receiver in a pseudolite navigation system, *Sensors*, 10, 6324-6346. <https://doi.org/10.3390/s100706324>
- Song, J.-H., Im, S.-H., & Jee, G.-I. 2013, Performance Evaluation of Vector Tracking Loop Based Receiver for GPS Anti-Jamming Environment, *Journal of Institute of Control, Robotics and Systems*, 19, 152-157. <https://doi.org/10.5302/J.ICROS.2013.19.2.152>
- Spilker, J. J. 1995, Vector delay lock loop processing of radiolocation transmitter signals, March 14 1995. US Patent 5,398,034
- Spilker, J. J. 1996, Fundamentals of signal tracking theory, *Progress in Astronautics and Aeronautics*, 163:245-328. <https://doi.org/10.2514/5.9781600866388.0245.0327>
- Won, J.-H. & Eissfeller, B. 2010, Effectiveness Analysis of Vector-Tracking-Loop in Signal Fading Environment, *Proc. NAVITEC2010, ESTEC, Noordwijk, The Netherlands*, Dec. 8-9, 2010. <https://doi.org/10.1109/NAVITEC.2010.5708014>
- Won, J.-H., Eissfeller, B., & Pany, T. 2011, Implementation, Test and Validation of a Vector-Tracking-Loop With the ipex Software Receiver, *Proc. ION GNSS-2011, Portland, OR*, Sept. 20-23, 2011, pp.795-802
- Won, J.-H., Pany, T., & Eissfeller, B. 2012, Characteristics of Kalman Filter for GNSS Signal Tracking Loop, *IEEE T-AES*, 48, 3671-3681. <https://doi.org/10.1109/TAES.2012.6324756>



Jong-Hoon Won received the Ph.D. degree in the Department of Control Engineering from Ajou University, Korea, in 2005. After then, he had worked with the Institute of Space Technology and Space Applications at University Federal Armed Forces (UFAF) Munich, Germany. He was nominated as Head of GNSS Laboratory in 2011 at the same institute, and involved in lectures on advanced receiver technology at Technical University of Munich (TUM) since 2009. He is currently an assistant professor of the Department of Electrical Engineering at Inha University. His research interests include GNSS signal design, receiver, navigation, target tracking systems and self-driving cars.



Wang-Seong Cheon received the MSc. Degree in the Department of Electrical Engineering from Inha University, Korea, in 2018. He is currently working with Hyundai Mipo Dockyard. His research interest includes GNSS signal processing and simulation.



Gun-Hoon Ji is currently in the undergraduate course in the Department of Electronics Engineering at Inha University, Korea. His research interests include GNSS receiver signal processing, navigation, and Vector tracking.

